Available online at www.sciencedirect.com
SCIENCE DIRECT®
ELSEVIER
Journal of Magnetism and Magnetic Materials 293 (2005) 473–482
Journal of magnetism and magnetic materials
www.elsevier.com/locate/jmmm

Doxorubicin magnetic conjugate targeting upon intravenous injection into mice: High gradient magnetic field inhibits the clearance of nanoparticles from the blood

Olga Mykhaylyk*, Nataliya Dudchenko, Alexandre Dudchenko

Institute for Applied Problems Physics & Biophysics, NAS, Sluzhbova 3, P.O.Box 355, UA-03142 Kyiv, Ukraine

Available online 2 March 2005

Abstract

The efficiency of a stationary magnetic field ($|\nabla B| = 200\,\mathrm{mT/cm}$) in increasing the bioavailability of a doxorubicin-magnetite nanoparticle conjugate (diameter of $24 \pm 19\,\mathrm{nm}$) in the mouse lung was determined by pharmacokinetic investigation using electron spin resonance (ESR). The magnetic field was also found to inhibit the elimination of nanoparticles from the blood and increase the conjugate half-life and bioavailability in the blood.

PACS: 87.83.+a; 87.68.+z; 87.50.Mn; 81.07.Bc; 87.64.Hd

Keywords: Magnetic drug targeting; Doxorubicin; Adriamycin; Drug-conjugate; Non-uniform magnetic field; Pharmacokinetics; Electron spin resonance (ESR); Nanodispersed magnetite; Hydroxyethylstarch; Polyethylene glycol (PEG)

1. Introduction

Much effort in research is directed toward finding less toxic and more efficient pharmaceutical formulations, especially for anticancer drugs. Conjugating some drugs to colloidal carriers has been shown to favorably influence their efficacy and toxicity [1]. For example, doxorubicin (DOX), known for its cardiotoxicity, bone marrow and gastrointestinal toxicity [2] was shown to be less toxic when associated with nanoparticles [3].

The idea of using magnetic colloidal materials as drug carriers controlled by an external magnetic field was first suggested long ago [4], and recently reviewed [5,6]. Optimization of the conditions for holding relatively large ($>1\,\mu\mathrm{m}$) magnetic microspheres [7,8] or a ferrofluid drop [9] in blood vessels has been undertaken previously. Complex hemodynamics, interaction of the magnetic nanoparticles with blood proteins and cells, and particle aggregation all contribute to the extremely

*Corresponding author. Institut für Experimentelle Onkologie und Therapieforschung TUM, Ismaninger Str. 22, D-81675 München, Germany. Tel.: +49 16095121846.
E-mail address: olga.mykhaylyk@gmx.net (O. Mykhaylyk).

0304-8853/$ - see front matter © 2005 Elsevier B.V. All rights reserved.
doi:10.1016/j.jmmm.2005.01.063

complex magnetohydrodynamics of magnetic drug targeting. In general, magnetic targeting efficiency is determined by the force applied to particles possessing a magnetic moment, and thus, increases with the increasing gradient of the magnetic field and the volume of the particles. The volume or dimension of the carriers has an upper limit imposed by limited permeability of the capillary bed. To penetrate through the blood vessel wall into the interstitium, conjugate particles should not be larger than 400–500 nm, taking into account that the capillary bed is generally permeable to particles smaller than 2 nm [10]. The bone marrow, liver, spleen and certain tumors are tissues with fenestrations of up to 150 nm in diameter [11]. Cut-off barriers of about 500 nm for macromolecular therapeutic access to tumor cells through endothelial gaps or transcellular holes have also been reported [12].

To trap insulated magnetite nanoparticles in the blood vessels, one would have to impose an extremely large magnetic field gradient. This problem is at least partially overcome by the reversible aggregation of magnetic particles [13,14]. The effective magnetic moment of the aggregates is significantly higher than that of an individual magnetic nanoparticle.

The objective of the present work was to look at the pharmacokinetics of a newly synthesized doxorubicin magnetic conjugate (DOX-M) with magnetite nanoparticles in a mouse model, and to test the efficiency of conjugate magnetic targeting in a non-uniform magnetic field. To accomplish this, we measured the efficient mobility of the conjugate aggregates in a range of field gradients. The magnetic field gradient to be applied for conjugate trapping in capillary vessels was also estimated, and the efficiency of these field gradients in conjugate targeting was quantitatively characterized in terms of relative conjugate bioavailability and the parameters of the two-compartment model for DOX-M pharmacokinetics.

2. Experimental

All chemicals were purchased from Sigma-Aldrich. Nanodispersed magnetite modified by hydroxyethylstarch was synthesized as described elsewhere [15] and activated with 1,6-diisocyanatohexane. The mean diameter of the particle magnetic core was 24 ± 19 nm according to transmission electron microscopy (TEM) data. The phase composition of the core was close to pure magnetite (99% magnetite + 1% α-FeOOH), and the saturation magnetization (134 ± 5 emu/g Fe) was close to that of the bulk magnetite (4.1 μ_B per formula unit or 138 emu/g Fe [16]).

To synthesize DOX-M conjugates, doxorubicin (DOX) was chemisorbed onto the surface of the activated nanocarrier from aqueous solution. Loading was 25.1 and 6.1 mg DOX per g of activated carrier for DOX-M1 and DOX-M2 conjugates, respectively. Iron content in the conjugates was 0.57 g Fe/g dry weight. The conjugates were stable, as less than 5% of chemisorbed DOX was released over 24 h when tested at 37 °C in a physiological solution, pH 7.4. The cytotoxicity of the DOX-M1 and DOX-M2 conjugates in vitro against the A2780 human ovarian carcinoma (IC_{50}s of 16.0 ± 0.1 and 2.3 ± 0.2 ng DOX/ml, respectively) and KB human epidermoid oral cavity cancer cell lines (IC_{50}s of 6.9 ± 0.1 and 9.0 ± 0.1 ng DOX/ml) was close to that of free DOX (IC_{50}s of 3.4 ± 0.2 and 6.4 ± 0.4 ng DOX/ml).

To determine the conjugate aggregates' efficient velocity (V_{eff}) at 37 °C in a hydroxyethylstarch plasma substitute, the optical density of the suspension after ultrasound treatment and magnetic field gradient application was measured in the center of the cuvette over time. The conjugate concentrations ranged from 0.04 to 0.33 g/l and the magnetic field gradients created perpendicular to the measuring laser beam ranged from 13 to 36 mT/cm. Efficient velocity was roughly estimated as $V_{eff} = L/t$, where $L = 13$ mm is the cuvette dimension in the direction of particle movement, and t is the time required for a 10-fold decrease in optical density to occur.

DOX-M conjugates were given as bolus injections of 0.1 ml suspensions into the eye sinus vein of adult male mice, each weighing approximately 20 g, in a dose of 12.5 μg Fe/g tissue (w/w) with no magnetic field applied (DOX-M1 and DOX-M2 series), with the magnetic field maximum centered over the left lung (DOX-M1_LG and

DOX-M2_LG series) or over the liver (DOX-M1_LV and DOX-M2_LV series). Animals from the reference group received 0.1 ml of physiological solution.

Animals were exposed to the magnetic field for 2 min or for 60 min for the 60, 180, and 1440 min time intervals between the introduction of the suspension and sacrifice of the animals. A non-uniform magnetic field was created by an electromagnet. The actual characteristics of the field applied to the animals are shown in Table 1. After sacrifice, blood, liver, spleen, left lung, kidney, and heart tissue samples were removed and quickly frozen in liquid nitrogen. Six animals were used for each series and exposure time and for the control group.

To study the pharmacokinetics of the carrier, the conjugate concentration was determined using magnetic resonance curves obtained from ESR spectra. The ESR spectra were obtained using an EPA-10 mini spectrometer (St. Petersburg Instruments, St. Petersburg, Russia) at 145 K. ESR spectra of the conjugate suspensions in a gelatine phantom were measured for calibration purposes (Fig. 1a). To determine the concentration of the conjugate in the blood and tissues of experimental animals (Figs. 1c and d), calibration curves were made by calculating the peak double integral intensity. A correction was made for background tissue absorption of the HF-radiation in the region of the magnetic carrier spectrum, and samples were taken from the control group of animals for every tissue type (*ref* curves in Figs. 1b and c). A sample of copper (II) sulfate in a water–glycerin medium (1:1) was used as a reference. Data were calculated as the mean of six measurements

Table 1
Characteristics of the magnetic field B (mT) and field gradient $/\nabla B/$ (mT/cm) applied to the tissues with no external magnetic field except that of the Earth (*ref* or DOX-M1 and DOX-M2 series), magnetic field maximum centered over the lung (*_LG series) or over the liver (*_LV series)

Tissue	Series					
	ref		*_LG		*_LV	
	B	$/\nabla B/$	B	$/\nabla B/$	B	$/\nabla B/$
Lungs	0.5	0	210	200	100	66
Liver	0.5	0	73	60	83	66
Spleen	0.5	0	73	40	95	60
Kidneys	0.5	0	73	40	87	47
Heart	0.5	0	112	90	65	33

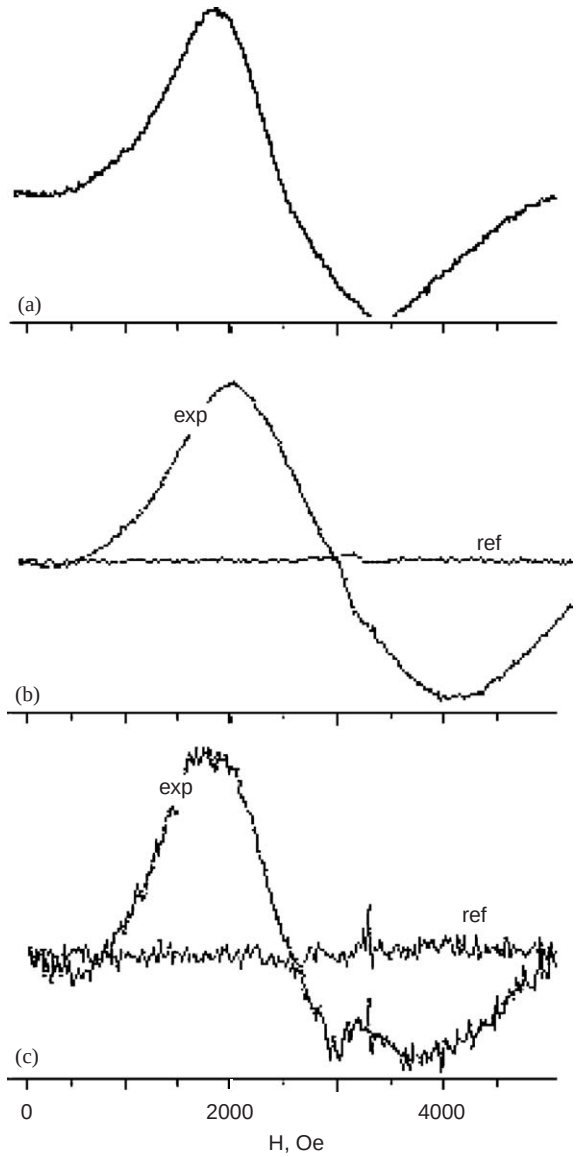

Fig. 1. ESR spectra for the DOX-M conjugate (*exp* curves) in a gelatin phantom (a), in the blood (b), and in the heart tissue (c), and background absorption of the tissues taken from the reference animals (*ref* curves in b and c): frequency 9.3 GHz; microwave power 20 mW; $T = 145$ K, modulation amplitude 10 G.

performed in six parallel probes from different animals for every four incubation time points. Data were presented in terms of relative bioavailability and area under the curve (AUC) of the conjugate concentration vs. time from the first time point (2 min) to the end point (1440 min or 24 h). Relative bioavailability was calculated as C/D, where C is the conjugate concentration in the tissue and D is a dose of the injected conjugate per unit of animal weight. To compare original data with the biodistribution profile of free DOX and DOX conjugate with polyisohexylcyanoacrylate nanoparticles (IHCA-DOX, 260 nm diameter), tissue distribution data, expressed in Ref. [17] as a percentage of the injected drug dosage in each organ $T(\%)$, were recalculated into the bioavailability index as follows: $C/D = T(\%)^{*}P/100^{*}P_{\text{organ}}$, where P is the average weight of the animal, and P_{organ} is the average weight of the organ.

To determine the ultrastructural location of the magnetic nanomaterial in animal tissues and to generate quantitative data on the particle distribution, TEM images of ultrathin tissue sections were taken on JEM-100C electron microscope. For stereological analysis, calculations were done on randomly selected fields using the semi-automatic unit for processing graphical images.

3. Results and discussion

To ensure trapping of the magnetic carrier at the vessel wall, the steady-state velocity of the aggregates in the blood under the applied magnetic field gradients (“magnetic responsiveness”), V, must be greater than the critical velocity $V_{\text{cr}} = \bar{U}d/L$ (Table 2), according to the following semi-empirical criterion: $V > V_{\text{cr}}/\sin(1-\lambda)\pi/2$, where d is the vessel diameter, L is the vessel length, $\bar{U}$ is the average blood flow velocity, and λ is the trapping efficiency, varying from 0 to 1. The higher the V_{eff} of the particles in the applied magnetic fields, the greater is λ. For example, at $V/V_{\text{cr}} = 2.2$, λ is 0.7. To achieve a λ of 0.9, it is necessary to ensure that the V_{eff} of aggregates in the applied field gradient exceeds the critical velocity V_{cr} by 6.4-fold.

The measured V_{eff} of the DOX-M conjugate particles/aggregates in the applied magnetic fields was found to depend on the field gradient and the concentration of magnetic particles in suspension, as shown in Fig. 2. Taking into account the conjugate dose injected (12.5 μg Fe/g animal weight or 250 μg Fe per mouse) and the Fe content in the conjugates (57%), assuming that the total blood volume was 5–6% of body weight (1–1.5 ml in a 20–25 g mouse), one can estimate the maximum possible conjugate concentration in the blood immediately after intravenous (i.v.) bolus injection as 0.33 g/l. In the tested conjugate concentration range up to 0.33 g/l and at a magnetic field gradient of $\nabla B = 3.6\,\text{T/m}$ ($B = 0.09\,\text{T}$), V_{eff} varied between 0.5×10^{-4} and 3.2×10^{-4} m/s and exceeded critical velocities calculated for capillary and tumor vessels (Table 2). In our experiments we tested a magnetic field with $\nabla B = 20\,\text{T/m}$ and $B = 0.21\,\text{T}$ in DOX-M trapping in the mice lungs.

The distribution profile of DOX-M shows that the maximum concentration of the conjugate

Table 2
Critical velocities of aggregate movement in the blood $V_{\text{cr}} = \bar{U}d/L$ estimated for various blood vessels with diameter d, length L, and average velocity of the blood flow $\bar{U}$ using data given in Refs. [18,19]

Vessel	d (m)	L (m)	$\bar{U}$ (m/s)	V_{cr} (m/s)
End venas	1.5×10^{-4}	1.0×10^{-2}	1.3×10^{-2}	2×10^{-3}
Arterioles	5.0×10^{-5}	1.5×10^{-3}	7.5×10^{-3}	2.5×10^{-4}
Venules	4.0×10^{-5}	1.5×10^{-3}	3.5×10^{-3}	9.3×10^{-5}
Main Venas	2.4×10^{-4}	0.1	1.5×10^{-2}	3.6×10^{-5}
Capillary	6.0×10^{-6}	6×10^{-4}	7×10^{-4}	7×10^{-6}
Lung capillary	8.0×10^{-6}	3×10^{-3}	1.43×10^{-3}	3.7×10^{-6}
Tumor vessels	$(5\text{–}50)\times10^{-6}$	3×10^{-3}	0.0001–0.0005	1.7×10^{-7}–8×10^{-6}

occurred in the liver, while the concentration of the carrier in the lungs was 2.5- to 5-fold lower. The total content of conjugate in the lungs was 0.03–0.06 that in the liver. The concentration of conjugate in the spleen was 2.5- to 3-fold lower than the concentration in the liver and close to that in the lungs. It is noteworthy that in all other tissues (heart, brain, kidneys, and especially muscle tissue) the conjugate concentration is very low. The AUCs of the carrier concentration are given in Table 3. The AUC values for lung tissue indicated that there was a significant difference between the two conjugate formulations. The observed accumulation of conjugate in the liver is a characteristic feature of all DOX forms in humans and animals [20].

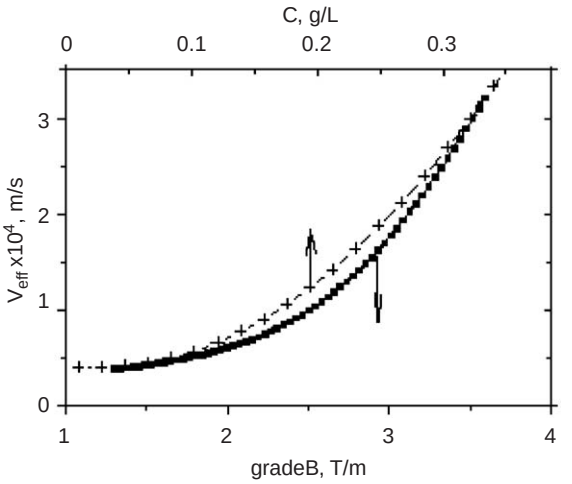

Fig. 2. Efficient velocity (V_{eff}) of the conjugate nanoparticles'/aggregates' movement in the 10% hydroxyethylstarch plasma substitute as a function of the magnetic field gradient (gradB, $C = 0.33$ g/l) and particle concentration (C, gradB $= 3.6$ T/m, $B = 0.09$ T), $t = 37 \pm 2$ °C.

In comparing our DOX-M conjugates to the literature data on free DOX and non-magnetic IHCA-DOX nanoparticles of similar size [17], the DOX-M conjugates exhibited a considerably modified distribution profile following i.v. injection. In particular, the liver and spleen retained more immobilized DOX, when associated with the magnetic carrier. DOX-M conjugates exhibited considerably less accumulation in the heart and kidneys compared to free DOX (Fig. 3). In general, this is a characteristic feature of nanoconjugates. The effect was much more pronounced for both tested DOX-M conjugates than for IHCA-DOX conjugate with non-magnetic nanoparticles (Fig. 3) and hence promises a reduction of the cardio- and nephrotoxicity compared to free DOX and reference IHCA-DOX conjugate.

Non-uniform magnetic field application ($B = 210$ mT and gradB $= 200$ mT/cm) was a potent factor in modifying DOX-M conjugate pharmacokinetics. Magnetic field application resulted in considerable enrichment of the lungs, and depletion of the liver, in magnetic carrier compared to the reference data without an applied

Table 3
Areas under the curves (2–1440 min) of the carrier concentration (mg Fe/g min) following intravenous injection of DOX-M1 and DOX-M2 conjugates into mice at a dose of 12.5 mg Fe/kg animal weight with no magnetic field applied (AUC_{ref}) and with a non-uniform magnetic field maximum centered in the area of the left lung (AUC_{LG}) and the ratio of the values (AUC_{LG} /AUC_{ref})

Compartment	DOX-M1			DOX-M2		
	mg Fe/g min			mg Fe/g min		
	AUC_{ref}	AUC_{LG}	AUC_{LG}/AUC_{ref}	AUC_{ref}	AUC_{LG}	AUC_{LG}/AUC_{ref}
Blood	0.23	2.6	11.4*	0.2	1.4	7.0*
Liver	390	322	0.8	347	118	0.3*
Spleen	156	221	1.4	201	102	0.5*
Lungs	136	418	3.1*	400	483	1.2
Kidney	1.2	10	8.7*	2.9	3.8	1.3
Heart	1.1	3.3	3.0*	0.6	2.5	4.2*
AUC^{lungs}/AUC^{liver}	0.35	1.3	—	1.2	4.1	—

*Statistically significant difference, $p < 0.05$.

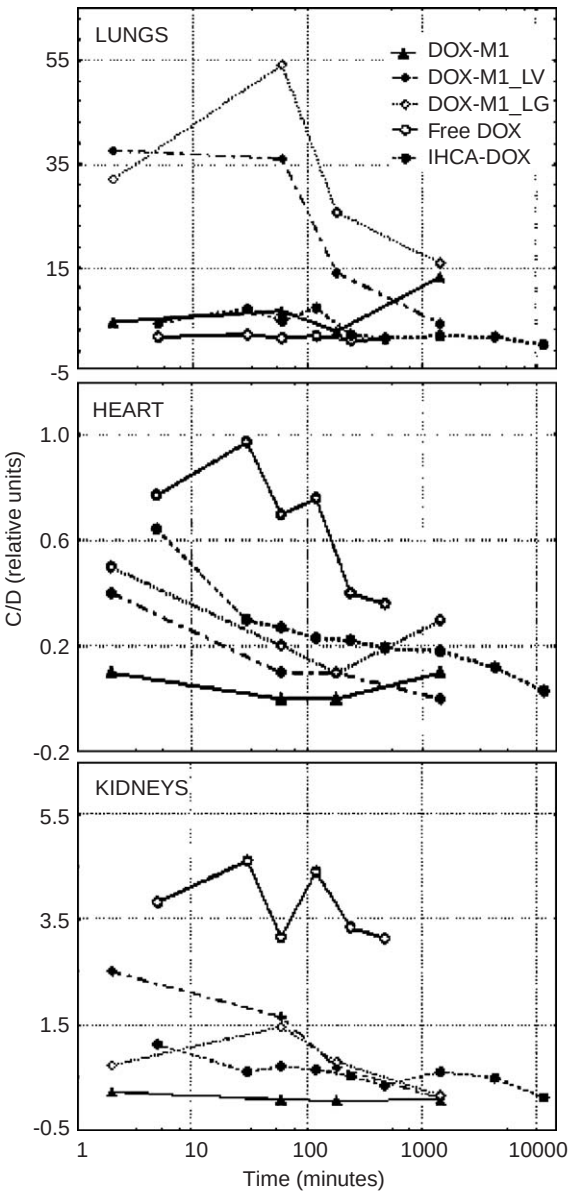

Fig. 3. Bioavailability (C/D) of the DOX-M1 conjugate (M, $n = 6$) in the lungs, heart and kidneys and following i.v. injection into mice. Values for Free DOX and IHCA-DOX conjugate were recalculated from Verdun et al. [20]. When used, the magnetic field maximum was applied over the lungs (DOX-M1_LG) or over the liver (DOX-M1_LV).

magnetic field (Table 2, Fig. 2). Increasing DOX-M1 bioavailability in the lungs correlated with the increasing gradient of the magnetic field applied to the lung tissue ($r = 0.9964$; $p = 0.05$). There was also a statistically significant increase in the accumulation of conjugate in kidney and heart tissue. As it is difficult to achieve good resolution in a mouse model, and despite the sharp field decay from the center to the periphery of the organs, the conjugate was captured in an effective "working zone", nevertheless, the bioavailability of the carrier still remains lower than for free DOX (Fig. 3).

The stereological data for TEM images are in agreement with the pharmacokinetic data concerning the considerable increase in conjugate bioavailability in the lungs under magnetic field application. Respiratory sections from the mouse lung (Fig. 4) show that after injection of the DOX-M1 conjugate, the number of particles (aggregates) per tissue unit volume was considerably higher under magnetic field application (2.72 ± 0.13 particles per μm^3) than in the absence of a magnetic field (0.69 ± 0.13 particles per μm^3; $t = 11.04$; $p < 0.01$). In terms of the volume of nanoparticles per tissue unit volume (%), this becomes - 0.63 ± 0.02 vs. 0.08 ± 0.02 ($t = 19.4$; $p < 0.01$) for the DOX-M1_LG and DOX-M1 series, respectively. Multiple particles were revealed in the nuclei of lymphocytes located in the capillary lumen and alveolar septum, and in the cytoplasm of alveolocytes, in the nuclei and cytoplasm of endotheliocytes, and in the blood capillary lumen.

Magnetic field effects on the pharmacokinetics of the magnetic conjugate in mice were not restricted to trapping at the target site. Statistically significant magnetic field inhibition of accumulation in the liver and spleen was detected for both conjugates after introduction of the suspension, coupled with considerably prolonged circulation in the blood (Fig. 5, Table 3). A positive correlation between the AUC in the blood and the gradient strength of the magnetic field applied to the liver was detected ($r = 0.9992$, $p = 0.025$ and $r = 1$, $p = 0.000$ for DOX-M1 and DOX-M2, respectively), whereas the AUC of the conjugate concentration in the liver negatively correlated with the strength of the magnetic field and field gradient applied to the tissue ($r = -0.9971$, $p = 0.049$ and $r = -0.9989$, $p = 0.030$).

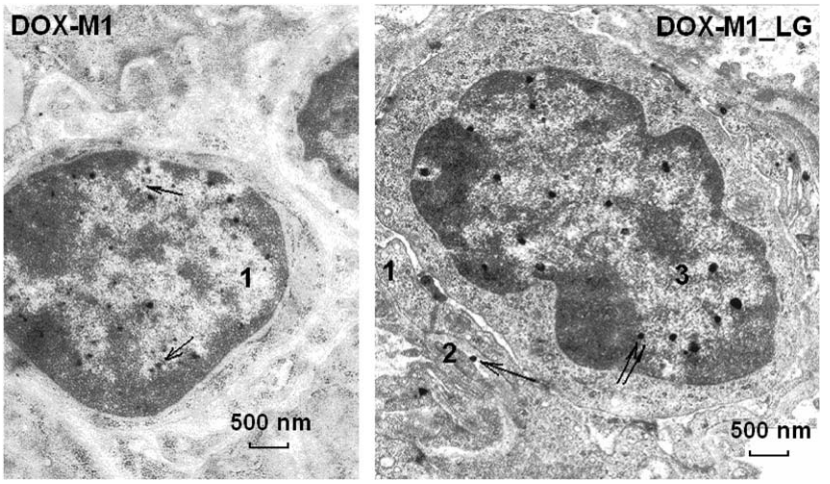

Fig. 4. Respiratory sections of mouse lungs 1 h after i.v. injection of the DOX-M1 conjugate without applied magnetic field (DOX-M1) and with magnetic field maximum imposed over the lungs (DOX-M1_LG). In the left panel, multiple nanoparticles (↑) were observed in the lymphocyte nucleus (1) in the alveolar diaphragm. In the right panel, conjugate nanoparticles (↑) were observed in the endotheliocyte cytoplasm (1), and basal membrane (2), and multiple particles (↑↑) were observed in the lymphocyte nucleus (3) located in the capillary lumen.

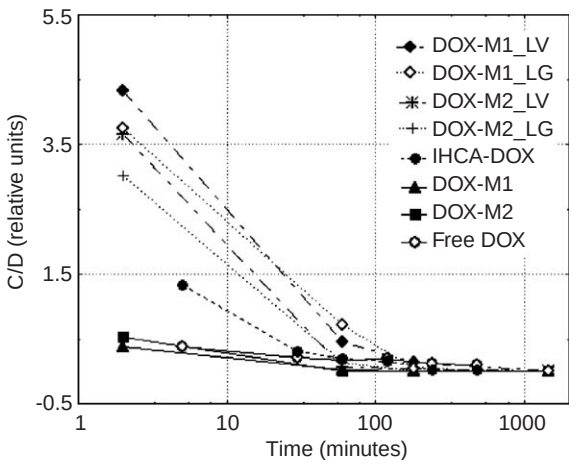

Fig. 5. Bioavailability (C/D) of the conjugates (M, $n = 6$) in the blood following i.v. injection into mice. Values are without (DOX-M1 and DOX-M2) and with the magnetic field imposed over the lungs (DOX-M1_LG and DOX-M2_LG) or over the liver (DOX-M1_LV and DOX-M2_LV). Values for Free DOX and IHCA-DOX conjugate were recalculated from Verdun et al. [20].

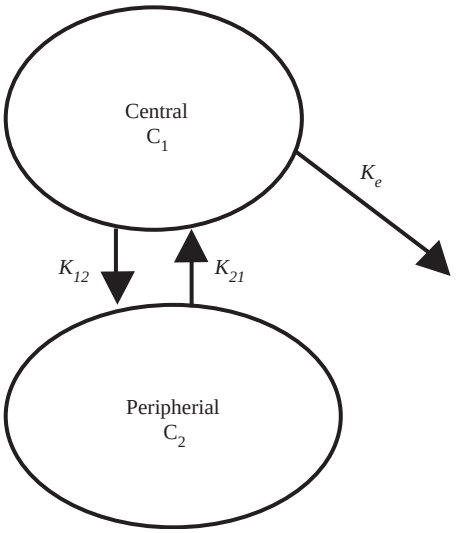

Fig. 6. Scheme for the two-compartment pharmacokinetic model.

The well-known two-compartment pharmacokinetic model (Fig. 6) with nest parameters can be used to analyze our data. The model is represented by the following equations:

$$C_1 = A_1 e^{-\alpha t} + B_1 e^{-\beta t}; \quad C_2 = A_2 e^{-\alpha t} + B_2 e^{-\beta t},$$

$$C_{10} = A_1 + B_1; \quad k_{21} = \frac{A_1\beta + B_1\alpha}{A_1 + B_1},$$

$$k_e = \frac{\alpha\beta}{k_{21}}; \quad k_{12} = \alpha + \beta - k_{21} - k_e,$$

where C_1 and C_2 are current preparation concentrations in central (first) and peripheral (second) cameras. C_{10} is the starting concentration of the preparation in the blood at $t = 0$. The speed constants, k_{12} and k_{21}, represent the preparation transfer from the first to the second camera and vice versa; k_e is the speed constant for preparation elimination from the first camera. The preparation is quickly distributed in a volume of distribution, $V_d = D/C_{10}$, which includes blood plasma and tissues with fast exchange of the preparation with plasma (central camera 1). Peripheral camera 2 includes tissues with slow exchange of the preparation. D is the dose.

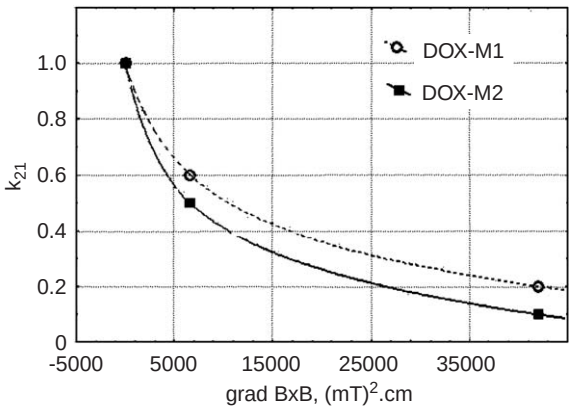

Fig. 7. Normalized speed constant (k_{21}) of the two-compartment model for pharmacokinetics of the DOX-M1 (○) and DOX-M2 (■) conjugates in mice vs. the product of the magnetic field and field gradients applied to the lungs.

The reverse transport of the carrier from the second to the first camera is inhibited by the magnetic field and the corresponding speed constant k_{21} decreases with increasing field and field gradient applied to the lungs (Fig. 7). This is reflected by the measured efficiency of the magnetic fields in trapping the conjugate in the lungs.

There are considerable increases in A_1 and B_1 parameters and decreases in α and β under magnetic field application (Table 4, Fig. 8). In other words, both fast and slow elimination half-lives, $t_{\frac{1}{2}}\alpha$ and $t_{\frac{1}{2}}\beta$, increase and the speed constant of preparation elimination from the first camera, k_e, decreases with increasing fields and field gradients. Correspondingly, the volume of distribution $V_d = D/C_{10}$ decreases substantially.

There is a large amount of data on the biological effects of magnetic fields, though most experimental efforts are focused on the effects of weak and low frequency magnetic fields. The effects of stationary strong magnetic fields in lowering the metabolic activity of HL-60 cells in vitro was observed only in cells exposed to a 1 T homogenous static magnetic field [21]. Moreover, in the only work published on the in vitro effects of strong magnetic fields on cellular immune

Table 4
Parameters of the two compartment model determined from the experimental data on carrier concentration in the blood following i.v. injection of DOX-M1 or DOX-M2 conjugates into mice with no magnetic field applied (DOX-M1 and DOX-M2 series) and with a non-uniform magnetic field maximum imposed over the lung (DOX-M1_LG and DOX-M2_LG series) or over the liver (DOX-M1_LV and DOX-M2_LV series)

Parameters of the model	Series					
	DOX-M1	DOX-M1_LG	DOX-M1_LV	DOX-M2	DOX-M2_LG	DOX-M2_LV
A_1(μg Fe/g w/w)	5.15	49.2	56.6	7.3	41.0	54.1
α (min$^-$)	0.08	0.03	0.05	0.07	0.06	0.10
B_1(μg Fe/g w/w)	0.19	0.53	2.72	0.02	0.16	0.63
β (min$^-$)	0.004	0.0008	0.002	0.004	0.00032	0.001
$t_{\frac{1}{2}}\alpha = 0.693/\alpha$ (min)	8.9	23.9	14.7	9.4	12.6	6.7
$t_{\frac{1}{2}}\beta = 0.693/\beta$ (min)	173	877	346	173	2154	693
C_{10} (μg Fe/ml)	5.3	49.7	59.3	7.3	41.1	54.7
k_{12} (min$^-$)	0.029	0.008	0.022	0.003	0.022	0.055
k_e (min$^-$)	0.047	0.021	0.023	0.071	0.033	0.048
k_{21} (min$^-$)	0.007	0.001	0.004	0.004	0.0005	0.002
$V_d = D/C_{10}$ (ml)	47	5	4	34	6	5

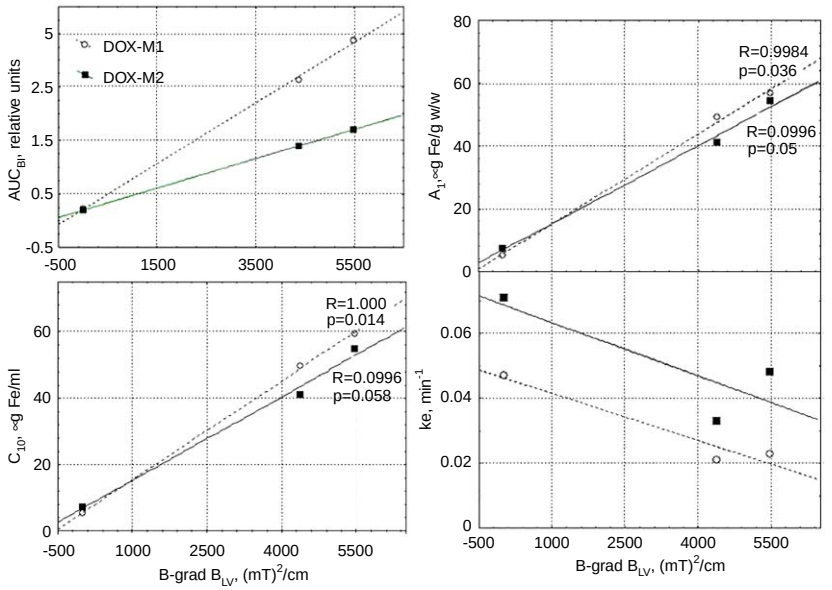

Fig. 8. Area under the curve values in the blood (AUC_{BI}) and the parameters of the two-compartment model for pharmacokinetics of the DOX-M1(○) and DOX-M2 (■) conjugates in mice vs. the product of the magnetic field and field gradients applied to the liver ($B\,\mathrm{grad}B_{LV}$).

Table 5
Morphometry data for ultra thin sections from mouse liver samples taken 1 h after i.v. injection of the DOX-M1 conjugate and with a magnetic field imposed over the lung (DOX-M1_LG): volume R_v (%) and number N_v (particles per μm^3) of the conjugate particles/aggregates in a unit of tissue or cell volume of the liver tissue, hepatocytes and Kupffer liver cells

Series	Index	Liver tissue	Hepatocytes	Kupffer cells	Ratio
DOX-M1	N_v	0.67 ± 0.14	0.56 ± 0.1	1.12 ± 0.3	2.0
	R_v	0.180 ± 0.050	0.099 ± 0.01	0.310 ± 0.106	3.1
DOX-M1_LG	N_v	$0.30\pm0.04^{*}$	$0.29\pm0.06^{*}$	$0.42\pm0.09^{*}$	1.4^{*}
	R_v	$0.052\pm0.007^{**}$	$0.055\pm0.01^{*}$	$0.067\pm0.016^{*}$	1.2^{*}

*Difference between series is statistically significant, $p<0.05$; **$p<0.01$.

parameters, exposure of murine macrophages, spleen lymphocytes, and thymic cells to 25–150 mT static magnetic fields resulted in decreases in the phagocytic activity of these cells [22].

Our data on the inhibition of the "swallow ability" of liver tissues with increasing magnetic field and/or gradients, resulting in a longer conjugate half-life in the blood, can be associated with the in vivo inhibition of the phagocytic activity of the immunocompetent cells. Morphometry data (Table 5) are in agreement with pharmacokinetic data and also reveal the decrease in conjugate concentration in the liver tissue and cells as well as the relative decrease in conjugate concentration in the Kupffer cells ("Ratio" column in Table 5).

4. Conclusions

The conjugation of doxorubicin with 30 nm magnetite core nanoparticles in the newly synthe-

sized DOX-M conjugates was shown to favorably influence DOX-M pharmacokinetics in mice after i.v. injection, compared to the pharmacokinetics of free doxorubicin. A non-uniform stationary magnetic field B of 0.21 T and ∇B of 20 T/m was shown to be efficient in DOX-M targeting in the mouse model. The inhibition of conjugate accumulation in the liver, upon application of magnetic fields B of 0.073 to 0.083 T and ∇B of 6 to 6.6 T/m to the liver, resulted in the increased bioavailability of the conjugates in the blood and could be used to modulate the pharmacokinetics of both magnetic and non-magnetic nanoparticles with immobilized drugs. This effect is worthy of a more detailed investigation.

Acknowledgments

We thank Dr. L. Stechenko for performing the electron microscopic studies. We also thank Dr. G. Solyanik for testing the anticancer activity of DOX conjugates in vitro, Dr. O. Stavinska and A. Chochlov for technical assistance, and Dr. J. Gerloff, Dr. A. Chubenko, and Dr. Lerman for valuable discussions.

References

[1] R. Dunkan, S. Dimitoijevic, E.G. Evagaron, STP Pharma. Sci. 6 (1996) 237.
[2] E.A. Lefrak, J. Ritha, S. Rosenheim, Cancer 32 (1973) 302.
[3] P. Couvreur, B. Kante, L. Grislain, et al., J. Pharm. Sci. 71 (1982) 790.
[4] K. Mosbach, U. Schröder, FEBS Lett. 102 (1979) 112.
[5] W. Schütt, C. Grüttner, U. Häfeli, et al., Hybridoma 16 (1997) 109.
[6] Q.A. Pankhurst, J. Connolly, S.K. Jones, et al., J. Phys. D.: Appl. Phys. 36 (2003) R167.
[7] K. Senyei, K. Widder, G. Czerlinski, J. Appl. Phys. 49 (1978) 3578.
[8] E.K. Ruuge, A.N. Rusetski, J. Magn. Magn. Mater. 122 (1993) 335.
[9] P.A. Voltairas, D.I. Fotiadis, L.K. Michalis, J. Biomech. 35 (2002) 813.
[10] E.M. Renkin, Circ. Res. 41 (1978) 735.
[11] L.W. Seymour, Crit. Rev. Ther. Drug Carrier Syst. 9 (1992) 135.
[12] F. Yuan, M. Dellian, D. Fukumura, et al., Cancer Res. 55 (1995) 3752.
[13] P.S. Scholten, J.A.P. Felius, J. Magn. Magn. Mater. 85 (1990) 107.
[14] D.A. Krueger, IEEE Trans. Magn. Mag- 16 (1980) 251.
[15] O. Mykhaylyk, A. Kotzuruba, O. Buchanevich, et al., J. Magn. Magn. Mater. 225 (2001) 226.
[16] R.M. Cornell, U. Schwertmann, in: R.M. Cornell (Ed.), The Iron Oxides: Structure, Properties, Reactions, Occurrences and Uses, Wiley-VCH, Weinheim, 2003.
[17] C. Verdun, F. Brasseur, H. Vranckx, et al., Cancer Chemother. Pharmacol. 26 (1990) 13.
[18] E.N. Lightfoot, Transport Phenomena in Living Systems. Biomedical Aspects of Momentum and Mass Transport, Wiley, New York, 1974.
[19] F. Yuan, H.A. Salehi, Y. Boucher, et al., Cancer Res. 54 (1994) 4564.
[20] H.S. Chen, J.F. Gross, Cancer Treat. Rep. 64 (1980) 31.
[21] J. Sabo, L. Mirossay, L. Hrovcak, et al., Bioelectrochemistry 56 (2002) 227.
[22] D. Flipo, M. Fournier, C. Benquet, et al., J. Toxicol. Environ. Health A 54 (1998) 63.